Biol Cybern (2005) 93: 463–470
DOI 10.1007/s00422-005-0020-1

ORIGINAL PAPER

Biological Cybernetics

C. Hauptmann · O. Popovych · P. A. Tass

Effectively desynchronizing deep brain stimulation based on a coordinated delayed feedback stimulation via several sites: a computational study

Received: 19 July 2004 / Accepted: 9 September 2005 / Published online: 21 October 2005

Abstract In detailed simulations we present a coordinated delayed feedback stimulation as a particularly robust and mild technique for desynchronization. We feed back the measured and band-pass filtered local field potential via several or multiple sites with different delays, respectively. This yields a resounding desynchronization in a naturally demand-controlled way. Our novel approach is superior to previously developed techniques: It is robust against variations of system parameters, e.g., the mean firing rate. It does not require time-consuming calibration. It also prevents intermittent resynchronization typically caused by all methods employing repetitive administration of shocks. We suggest our novel technique to be used for deep brain stimulation in patients suffering from neurological diseases with pathological synchronization, such as Parkinsonian tremor, essential tremor or epilepsy.

1 Introduction

Pathological synchronization is a hallmark of several neurological diseases like Parkinson's disease (PD) or essential tremor (Alberts et al. 1969; Nini et al. 1995). For example, Parkinsonian resting tremor is caused by a pacemaker-like population of neurons which fires in a synchronized and periodical way (Alberts et al. 1969). In contrast, in healthy subjects these neuronal populations fire in an uncorrelated, i.e. desynchronized manner (Nini et al. 1995). In patients who do not respond to drug therapy, electrical deep brain stimulation (DBS) is administered via depth electrodes chronically implanted in the thalamic ventralis intermedius nucleus or the subthalamic nucleus (Benabid et al. 1991, 2002). To this end, a permanent high-frequency (>100 Hz) periodic pulse train stimulation is used.

The mechanism of high-frequency DBS is not yet sufficiently understood. High-frequency DBS basically mimics the effect of tissue leasoning and appears to block neuronal activity in relevant target areas (Benabid et al. 2002). High-frequency DBS is the standard therapy for medically intractable patients suffering from Parkinson's disease and essential tremor. Standard DBS (SDBS) has been developed empirically, mainly based on experimental results and clinical observations. However, in some patients DBS may not help, or may cause side effects, or the therapeutic effects may disappear over time (Volkmann 2004). To find milder and more effective DBS techniques, a model-based development of novel stimulation protocols has been initiated (Tass 1999, 2002a,b, 2003a). For this, relevant target areas were modeled mathematically and novel stimulation techniques have been developed using stochastic phase resetting principles (Tass 1999).

In a first clinical study performed during electrode implantation, we have shown that the coordinated reset via several sites can suppress the peripheral tremor, even if the standard high-frequency DBS has no tremor suppressive effect (Tass et al. 2005). To achieve a coordinated reset of neural subpopulations one administers short high-frequency pulse trains via N stimulation sites, with a delay of T/N between the different resets. T approximates the mean period of the rhythm which has to be desynchronized. The coordinated reset splits a large synchronized population into a so-called N-cluster state, i.e. into N subpopulations, where the mean phases of the subpopulations are equally spaced within a unit cycle $[0, 2\pi]$. In the course of the resynchronization, when the stimulation is off, the neuronal population transiently passes through a desynchronized state. Hence, to maintain a desynchronized firing, a coordinated reset has to be performed repetitively. The disadvantage of this approach is that a desynchronized state cannot be maintained in a stable way. Rather, due to the repetitive stimulus administration, the neuronal population bounces between an N-cluster state and an

C. Hauptmann (✉) · O. Popovych · P. A. Tass
Institute of Medicine and Virtual Institute of Neuromodulation,
Research Center Juelich, 52425 Juelich, Germany
E-mail: c.hauptmann@fz-juelich.de

P. A. Tass
Department of Stereotaxic and Functional Neurosurgery,
University Hospital, 50924 Cologne, Germany

in-phase synchronization, spending most of the time in the transient desynchronized state in between.

In this paper we present a technique for the desynchronization of a strongly synchronized target population, where the desynchronized state is permanently and robustly maintained in a stable way without intermittent occurrence of resynchronization. The idea of the novel stimulation technique is as follows. In principle, perfect desynchronization can be achieved by stimulating all neurons individually, each with its own electrode and its own resetting stimulus (Tass 2003a). Stimulation signals which are appropriate to reset a single neuron are single pulses or pulse trains (Tass 2003a,b) as well as smooth signals such as sine waves (Tass 2002a). However, stimulating thousands of neurons, each with its own electrode, would damage the tissue and is, hence, not practicable. Nevertheless, we can approximate an individual control mode by a stimulation via several or multiple sites, where the stimulation via multiple sites might be realized by neurochip technology. For the sake of simplicity let us first consider a sinusoidal signal. It provides us with a soft control of the phase of the neuron, such that there is no strong perturbation of the frequency of the neuron, but an individual phase shift is induced (Richardson et al. 2003). Furthermore, if these harmonic signals are presented at different sites within the population they superpose, each neuron receives a combination of all these stimulation signals. These superposing signals form a new stimulation signal with a new phase shift for each neuron individually. For example, if two sinusoidal signals $S_1(t) = A_1 \sin(\omega t + \theta_1)$ and $S_2(t) = A_2 \sin(\omega t + \theta_2)$, with phase shifts θ_1 and θ_2, are superposed, we get $S_1 + S_2 = A \sin(\omega t + \theta)$ with $A = \sqrt{A_1^2 + A_2^2 + 2A_1A_2 \cos(\theta_2 - \theta_1)}$ and $\tan\theta = (A_1 \sin\theta_1 + A_2 \sin\theta_2)/(A_1 \cos\theta_1 + A_2 \cos\theta_2)$, which results in a new sinusoidal signal with a new phase shift. Figure 1 illustrates the effect of the superposition of the stimulation signals. Two electrodes deliver signals with different phases, so that each neuron is reseted by a combined stimulation signal with its own individual phase depending on the location of the neuron with respect to the stimulation electrodes.

Next, we have to choose appropriate stimulation signals instead of the rigid sine signals used for the illustration above.

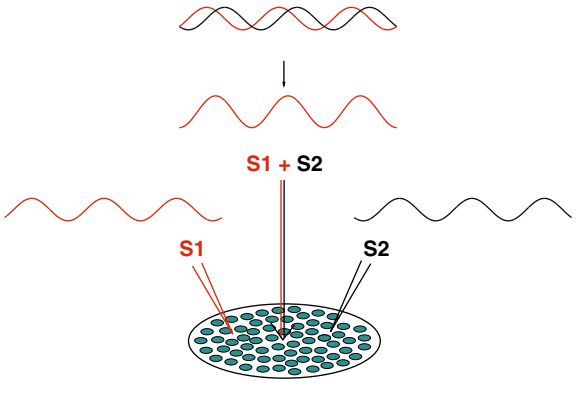

Fig. 1 The superposition of stimulation signals $S1$ and $S2$ creates stimulation signals with spatially varying phase shifts

Superposition-induced desynchronization can elegantly be realized in a demand-controlled way by using the delayed band-pass filtered local field potential (LFP) as stimulation signal. For this, the LFP has to be measured, amplified and feedback into the target population with different time delays via different stimulation sites, respectively. Strong synchronization of the target population leads to large variations of the LFP and, consequently, to strong stimulation signals. In contrast, in the case of an uncorrelated firing, the LFP has small variations, especially if a large number of neurons contribute to the LFP so that practically nothing is fed back. This realizes a demand-controlled stimulus administration in a natural way.

Below we consider stimulation protocols with four stimulation sites such that the LFP is fed back with four different time delays separated from each other by $T/4$, where T is close to the mean period of the oscillatory neurons. We demonstrate the novel stimulation technique by applying it to a mathematical model which accounts for the important dynamical properties of the neuronal target population.

2 Mathematical model

We use a microscopic model which is based on physiology. The model mimics the dynamical behavior of a population of neurons of the *subthalamic nucleus* (STN), displaying an oscillatory activity which is characteristic for Parkinson's disease (Nini et al. 1995). We use the well known Morris-Lecar equation as spike generator (Morris and Lecar 1981). In dimensionless form the dynamics of the membrane potential v_j of the jth neuron is described by the following set of equations

$$C\frac{dv_j}{dt} = -g_{ca}m_{\inf}(v_j)(v_j - v_{ca}) - g_k w_j(v_j - v_k) - g_l(v_j - v_l) + I_j, \quad (1)$$

$$\frac{dw_j}{dt} = \phi\frac{[w_{\inf}(v_j) - w_j]}{\tau_w(v_j)}, \quad (2)$$

with $m_{\inf}(v) = 0.5[1+\tanh\{(v-v_1)/v_2\}]$, $w_{\inf}(v) = 0.5[1+\tanh\{(v-v_3)/v_4\}]$ and $\tau_w(v) = 1/\cosh\{(v-v_3)/(2v_4)\}$. The parameters C, g_{ca}, g_k, g_l, v_{ca}, v_k, v_l, ϕ, v_1, v_2, v_3, and v_4 are adjusted following (Rinzel and Ermentrout 1989) and listed in the caption of Fig. 2. The external current I_j is composed out of a slow varying current I_j^{slow} important for the generation of bursting activity, a noise component I_j^{noise}, a current due to synaptical coupling I_j^{syn} and a stimulation current I_j^{stim}.

A slowly varying current I_j^{slow} which has been proposed by Rinzel and Ermentrout (1989) as a source of bursting behavior is introduced $\frac{dI_j^{\text{slow}}}{dt} = \epsilon[(v^\star - v_j(t-\tau_i)) - \alpha I_j^{\text{slow}}]$, where $v^\star$, ϵ, and α are parameters. This models the inhibitory feedback from the globus pallidum exterior (GPe). The neurons in this area are excited by the STN activity and, with a time delay τ_i, the inhibitory effects from the GPe result in an inhibition in (1) (Hauptmann and Mackey 2003). Noise introduced by external and internal sources is modeled by

a spatially incoherent exponentially correlated noise source I_j^{noise} (Dolan et al. 1999). A constant current I_j^{const} adjusts the spike generator with respect to the onset of oscillatory behavior necessary for the bursting activity.

The neurons within the STN are coupled by excitatory synapses. The synaptic interaction is modeled as suggested by Terman et al. (2002). The post-synaptic effect of an action potential spreading from neuron k is calculated at the source neuron side. The action potential results in an opening of the corresponding ion gates according to $\frac{dg_k^s}{dt} = \alpha_s \frac{1}{1+e^{-(v_k-\theta_s)/\sigma_s}} (1 - g_k^s) - \beta_s g_k^s$, where α_s, θ_s, σ_s, and β_s are parameters listed in the caption of Fig. 2. The local gating variables g_k^s are weighted with a distance-dependent function and are multiplied with a maximal gating term and the potential difference corresponding to the glutamatergic synapses present in the STN. The resulting synaptic current $I_j^{\text{syn}}(t)$ driving the jth neuron is given by $I_j^{\text{syn}}(t) = \bar{g}_s(v_j - v_s)\frac{c_1}{N\sqrt{2\pi}\sigma_g} \sum_k \exp -\frac{||\mathbf{x_j}-\mathbf{x_k}||^2}{2\sigma_g^2} g_k^s(t)$, where $||\mathbf{x_j} - \mathbf{x_k}||$ is the distance between the kth and the jth neuron. c_1 is a normalization factor and $\bar{g}_s$, v_s, and σ_g are parameters. N is the number of neurons in the population. The details of connections within the populations on which most of the current studies of Parkinsonian disease focus, the basal ganglia, are poorly understood (Terman et al. 2002). However, from other areas we know that rather local than global connections are realized (Traub and Miles 1991; Hellwig 2000).

The stimulation is formed by the band-pass filtered and time delayed LFP detected by a center electrode (see Fig. 2a). The LFP $V^f(t) = \frac{R_e}{4\pi} \sum_{j=1}^{N} \frac{I_j(t)}{r_j}$ is calculated using the method proposed by Nunez (1981), where r_j is the distance between neuron j and the recording electrode, $I_j(t)$ are the ionic currents defining the dynamical behavior of neuron j, see (1). R_e is the extracellular resistivity, which is assumed to be homogeneous. The LFP is band-pass filtered by using a damped harmonic oscillator.

In our stimulation protocols, the stimulation is administered via four electrodes located within the network. The time delay is related to the mean period T of the neural activity. The resulting effect of the stimulation $I_j^{\text{stim}}(t)$ on the jth neuron induced by the four electrodes is given by $I_j^{\text{stim}}(t) = c_s X(t) \sum_{k=1}^{4} e^{-2||\mathbf{x_j}-\mathbf{X^k}||} \tilde{V}_k^f(t - \tau_k)$, where $||\mathbf{x_j} - \mathbf{X^k}||$ is the distance between the kth electrode and jth neuron, and c_s is the parameter which controls the strength of the stimulation. $X(t)$ determines the onset and offset of the stimulation and $\tilde{V}_k^f(t - \tau_k)$ is the time delayed (delay τ_k) and band-pass filtered LFP presented through the kth electrode. The external currents $I_j(t)$ for the jth neuron in (1) are given by $I_j(t) = I_j^{\text{slow}} + I_j^{\text{noise}}(t) + I_j^{\text{const}} + I_j^{\text{syn}}(t) + I_j^{\text{stim}}(t)$.

In the stimulation protocols below we consider a setup, where a strongly synchronized neuronal population (population 1) acts as a pacemaker and drives another population (population 2), which gets synchronized only because of the driving. For example, the pacemaker-like population in the basal ganglia and thalamus drives cortical motor areas which

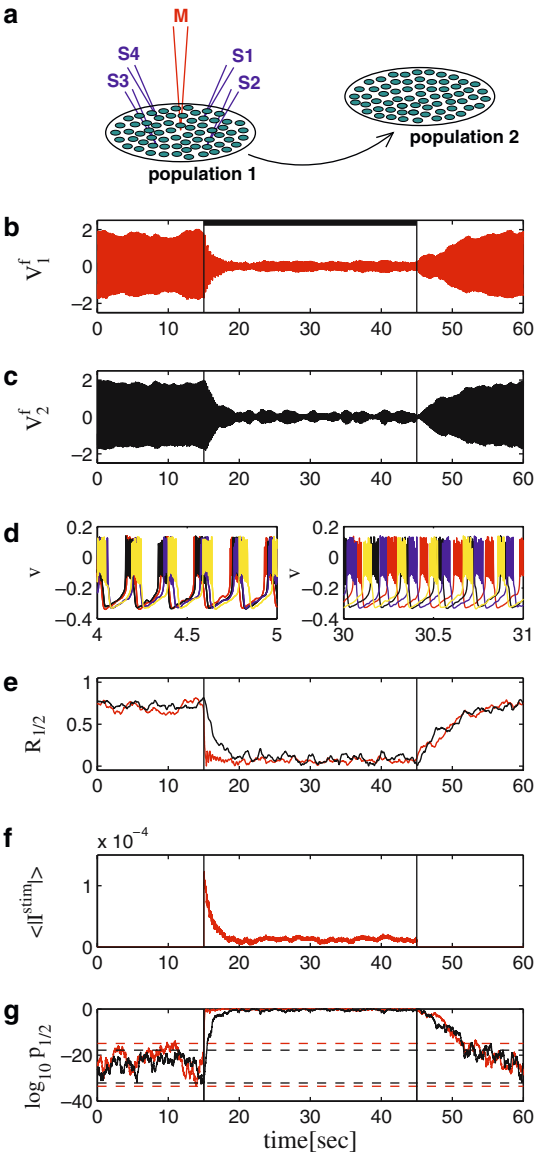

Fig. 2 First stimulation protocol: The LFP is measured in population 1 which is permanently stimulated by the delayed feedback stimulation during $t \in [15, 45]$. **a** Schematic plot of the stimulation setup. **b** LFP of population 1. **c** LFP of population 2. **d** Membrane potentials of four representative neurons of population 2 before stimulation (*left*) and during stimulation (*right*). **e** Synchronization measure R of population 1 (R_1, *red*) and 2 (R_2, *black*). **f** Mean stimulation current. **g** Logarithmic plot of the p-value of the Kuiper test of population 1 (p_1, *red*) and 2 (p_2, *black*). Lower and upper dashed lines indicate the corresponding 1st and 99th percentile of the corresponding prestimulus distribution $[-10, 15]$. **b,c,e–g** *Vertical lines* indicate onset and offset of the stimulation. Parameters: $N_1 = 100$, $N_2 = 100$, $g_{ca} = 1.0$, $g_k = 2.0$, $g_l = 0.5$, $v_{ca} = 1.0$, $v_k = -0.7$, $v_l = -0.5$, $v_1 = -0.01$, $v_2 = 0.15$, $v_3 = 0.1$, $v_4 = 0.145$, $C = 1.0$, $\phi = 1.15$, $\epsilon = 0.002$, $v^\star = -0.22$, $\alpha = 0.0$, $\tau_i = 10$, $I_j^{\text{const}} = 0.075$, $\sigma_g = 0.5$, $D_{\text{noise}} = 0.00001$, $\alpha_s = 0.1$, $\beta_s = 0.05$, $\theta_s = 0.2$, $\sigma_s = 0.02$, $\bar{g}_s = 0.4/0.05$, $v_s = -0.85$, $R_e = 1$, $\tau_1 = 0.125T$, $\tau_2 = 0.375T$, $\tau_3 = 0.625T$, $\tau_4 = 0.875T$ (T = mean period of the system), $c_1 = 2.1765$, $c_s = 0.011$, $X(t) = 1$ for $t \in [15, 45]$ and $X(t) = 0$ otherwise, $t_a = -10$, $t_b = 15$

induce the peripheral shaking (Volkmann et al. 1996). We model two neuronal populations (Fig. 2a): A driver (pacemaker) and a population (cortex) driven by the pacemaker via synaptic connections. Within each population the coupling is local, respectively, whereas the coupling strengths between the two populations are randomized and obey a Gaussian distribution. To study the challenging situation of strong driving, we assume that the mean coupling within the driving population is equal to the mean coupling between the two populations. The excitatory coupling between pacemaker and driven system is given by $\bar{g}_s = 0.4$. Within the driven population weak excitatory synaptic coupling exists, which by itself does not induce synchronization ($\bar{g}_s = 0.05$). For illustration, we represent the neurons in the populations as arranged in square lattices and four stimulation electrodes are equally spaced within the population. The fifth measuring electrode is positioned in the center of the neuron population (Fig. 2a).

3 Results

We define the phase $\Phi_j(t)$ of the individual neuron j by standard interpolation (Pinsky and Rinzel 1995): $\Phi_j(t) = 2\pi \frac{t-t_k}{t_{k+1}-t_k}$, where $t \in [t_k, t_{k+1}]$, and t_k is the onset time of the kth burst of the neuron. The phases enable us to assess the extent of in-phase synchronization of a population with the standard order parameter $R(t) \exp[i\Theta(t)] = \frac{1}{N}\sum_{j=1}^{N} \exp[i\Phi_j(t)]$, where R is the synchronization measure and Θ is the mean phase (Kuramoto 1984). $0 \leq R(t) \leq 1$ for all times t, where complete absence of in-phase synchronization corresponds to $R = 0$, whereas perfect in-phase synchronization is characterized by $R = 1$.

Another quantity for the characterization of synchronous dynamics is the Kuiper test which is a circular version of the Kolmogorov–Smirnov test. For a given distribution of phases $\{\Phi_1, \ldots, \Phi_N\}$ at time t it provides us with the probability $p(t)$ (the so-called p-value), with which $\{\Phi_1, \ldots, \Phi_N\}$ has to be considered as a uniform distribution (Kuiper 1960; Batschelet 1981). If $p = 1$, $\{\Phi_1, \ldots, \Phi_N\}$ is a uniform distribution and there are no synchronized or clustered states whatsoever, cluster states may not be detected by the standard order parameter R (Tass 1999). If p is close to 0, the neuronal population is synchronized, in-phase or in a cluster state. The first and the 99th percentile of the prestimulus distributions $\{p(t)\}_{t\in[t_a,t_b]}$ provide confidence levels, which allows one to determine whether a stimulus causes a significant change of the corresponding distribution of the phases.

The mean stimulation current is calculated by averaging the absolute values of the stimulation currents over the whole ensemble of N neurons $< |I^{\text{stim}}(t)| >= \frac{1}{N}\sum_{j=1}^{N} |I_j^{\text{stim}}(t)|$. Below we describe four exemplary stimulation protocols for the desynchronization of the strongly synchronized neural populations.

1. Desynchronization of the pacemaker using its LFP (Fig. 2): The synchronization in the pacemaker is caused by a strong excitatory coupling within the population. The LFP used for stimulation is measured within the pacemaker (Fig. 2a). The vertical bars indicate the on- and offset of the stimulation. The stimulation causes an instantaneous desynchronization of population 1, which shows up as a decrease of its LFP (Fig. 2b), a suppression of the synchronization measure R (Fig. 2e), and p-values close to 1 (i.e. $\log_{10} p$ close to 0) indicate an optimal, nearly uniform desynchronization (Fig. 2g). Due to missing synchronized synaptical input from the desynchronized population 1, population 2 gets desynchronized, too (Fig. 2c,e,g). The mean stimulation current plotted in Fig. 2f approaches zero because of its direct relation to the LFP of population 1: A weak stimulation input is sufficient to prevent the desynchronized population 1 from resynchronization. Note, the stimulation does not influence the bursting activity of the neurons (Fig. 2d). A decisive disadvantage of this stimulation protocol is the simultaneous stimulation, measurement and LFP recording at nearby sites. In experiments, the stimulation current exceeds the measured currents by a factor of 10^6. Consequently the LFP can be corrupted by stimulation artifacts and it might be difficult to use it as a feedback signal. We here present two methods in order to overcome this obstacle.

2. Desynchronization of the pacemaker using the LFP of the driven population (Fig. 3):

The first method simply uses the LFP of the driven population as feedback signal (Fig. 3a). The local separation of stimulation and recording sites guarantees that the feedback signal is not corrupted by stimulation artifacts. Nevertheless the stimulation effect is as good as in Fig. 2.

3. Desynchronization of the pacemaker by intermittent stimulation with its own LFP (Fig. 4): We propose another method to overcome the obstacle of protocol 1. Stimulation and

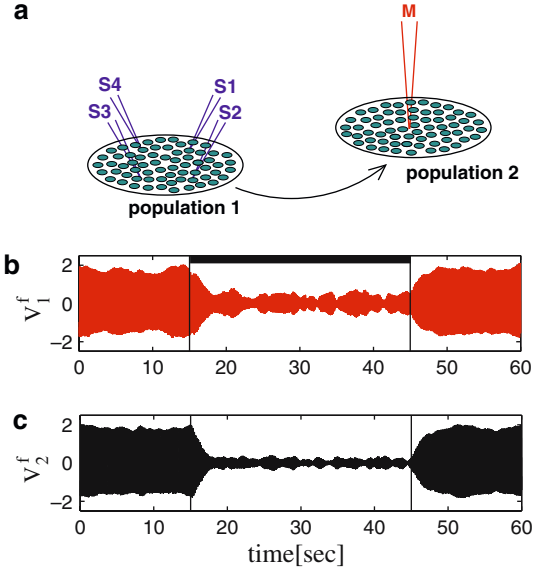

Fig. 3 Second stimulation protocol: The LFP is measured in population 2. Population 1 is permanently stimulated by the delayed feedback stimulation during $t \in [15, 45]$. **a** Schematic plot of the stimulation setup. **b** LFP of population 1. **c** LFP of population 2. The synchronization measures R and the p-values of the Kuiper test show similar behavior as in Fig. 2. Parameters are as in Fig. 2

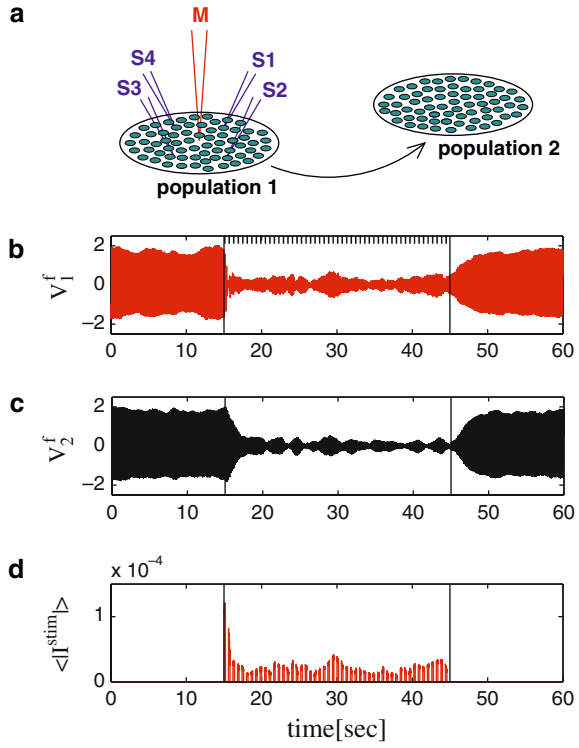

Fig. 4 Third stimulation protocol: The LFP is measured in population 1 which is intermittently stimulated by the delayed feedback stimulation during $t \in [15, 45]$. **a** Schematic plot of the stimulation setup. **b** LFP of population 1. **c** LFP of population 2. **d** Mean stimulation current. R and the p-values of the Kuiper test are similar to Fig. 2. The time delays are extended to $\tau_1 = 0.125T + T$, $\tau_2 = 0.375T + T$, $\tau_3 = 0.625T + T$, $\tau_4 = 0.875T + T$ ($T = 200$ ms: mean period of the system). Other parameters are as in Fig. 2

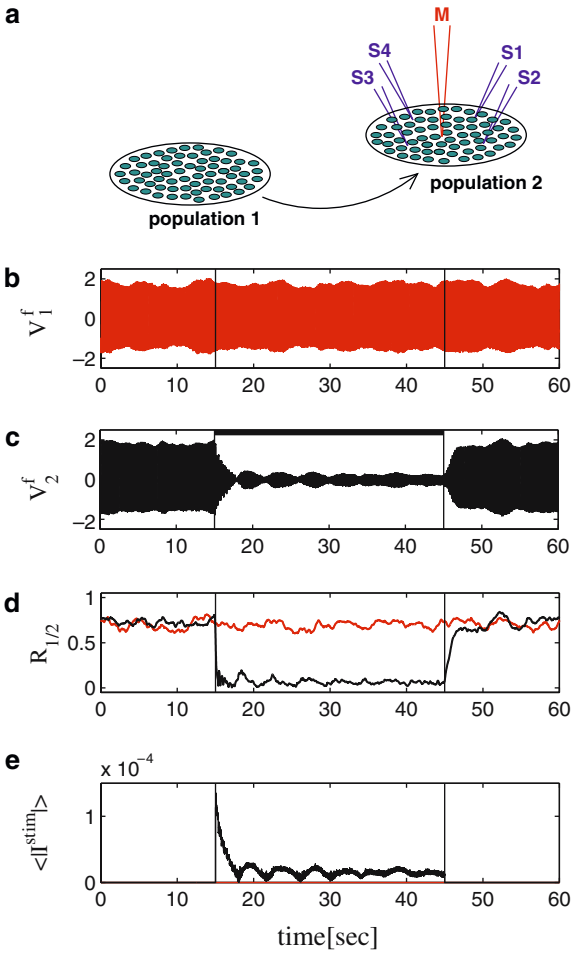

Fig. 5 Fourth stimulation protocol: The LFP is measured in population 2 which is permanently stimulated by the delayed feedback stimulation during $t \in [15, 45]$. **a** Schematic plot of the stimulation setup. **b** LFP of population 1. **c** LFP of population 2. **d** Synchronization measure R of population 1 (R_1, *red*) and 2 (R_2, *black*). **e** Mean stimulation current. Parameters are as in Fig. 2

recording are no longer performed simultaneously, but consecutively in a periodical manner: The stimulation is applied during short intervals without parallel measurement. These stimulation epochs are preceded by longer measurement intervals during which no stimulation is performed (Fig. 4). Note that the time delays cannot be smaller than the duration of the stimulation intervals. Even though stimulation is repetitively presented for 200 ms, each time preceded by a measurement period of 400 ms (Fig. 4), good desynchronization is achieved. Moreover, due to this intermittent type of stimulation the total stimulation current used is nearly three times lower than the total stimulation current used in the protocol of Fig. 2. If the length of the measurement periods is short compared to the time scale of the resynchronization, no significant resynchronization occurs during these periods (Fig. 4).

4. Desynchronization of the driven neuronal population using its own LFP (Fig.5): We apply the technique from Fig. 2 directly to the driven population. This is to demonstrate that our stimulation technique does not require that we stimulate the pacemaker directly. Rather we can also effectively desynchronize a neuronal population, which is driven by the pacemaker, by only stimulating the particular driven population. To avoid stimulation artifacts of the feedback signal, in medical applications one has to perform an intermittent stimulation (as in Fig. 4) or one has to use the LFP of another driven population, situated further downstream.

Let us compare our four stimulation protocols presented in this paper with the clinically established SDBS, i.e. the permanent high-frequency deep brain stimulation (Fig. 6). For the SDBS no measuring electrode and only one stimulation electrode is used. The stimulation electrode is optimally positioned in the center of population 1. As in the previous protocols the stimulation acts directly on the spike generator of the neurons, see (1). We use mono-phasic pulses of 0.2 ms duration. The pulses are interseced by pauses of 7.5 ms which results in a stimulation frequency of 130 Hz. The level of desynchronization induced by SDBS is lower compared to the stimulation protocols above (Fig. 6). Moreover, SDBS destroys the normal activity of the neurons and results in an irregular firing of the stimulated neurons, where the main activity pattern of the neurons is a spiking/bursting activity

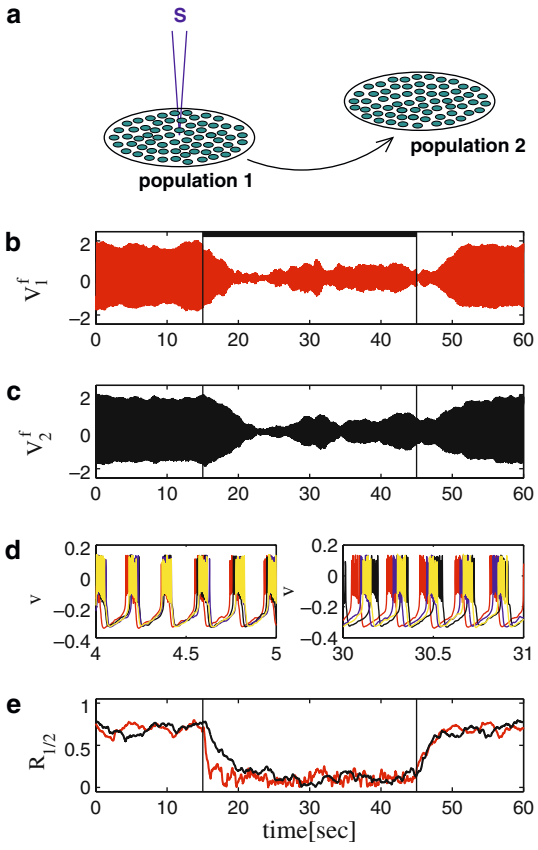

Fig. 6 Standard high-frequency stimulation. The stimulation amplitude is the same as used for Figs. 2 to 4. Population 1 is stimulated by the high-frequency pulse train (pulse duration 0.2 ms, frequency 130 Hz) during $t \in [15, 45]$. **a** Schematic plot of the stimulation setup. **b** LFP of population 1. **c** LFP of population 2. **d** Membrane potentials of four representative neurons of population 2 before stimulation (*left*) and during stimulation (*right*). **e** Synchronization measure R of population 1 (R_1, *red*) and 2 (R_2, *black*). The p-values of the Kuiper test are similar to Fig. 2. Other parameters are as in Fig. 2

with only one or two spikes per burst instead of typically 5–6. The neurons cannot follow the high-frequency activation because the slowly varying current I_j^{slow} mimicking the recurrent inhibition from GPe, prevents entrainment. SDBS results in a large mean stimulation current.

All the four presented stimulation protocols cause a desynchronization of the driven population. To compare the effectiveness of these stimulation protocols as well as SDBS, the time-averaged mean stimulation current is calculated (Table 1).

The mean p-value of the Kuiper test and the mean value of the synchronization measure R (low values indicate good performance) are evaluated and averaged in the time window $t \in [20, 45]$. The 5 sec directly after the stimulation onset are discarded. The first stimulation protocol from Fig. 2, indicated as stim 1, causes a very good desynchronization at very low stimulation current. The performance of the second and fourth stimulation protocols, indicated as stim 2 and stim 4 respectively, is even better, while using similar stimulation

Table 1 Evaluation of the desynchronization within population 2 during stimulation ($t \in [20, 45]$)

	Averaged stimulation current	Mean Kuiper index (pop. 2)	Mean R (pop. 2)
Stim 1	1.2×10^{-5}	−0.455	0.094
Stim 2	1.2×10^{-5}	−0.336	0.079
Stim 3	0.64×10^{-5}	−0.491	0.093
Stim 4	1.4×10^{-5}	−0.248	0.061
SDBS	25.9×10^{-5}	−0.782	0.124

The averaged stimulation current (mean stimulation current summarized over time and the stimulated neurons), the mean p-value of the Kuiper test for population 2 and the mean synchronization measure R of population 2 are listed. The labels stim 1 to stim 4 indicate the corresponding stimulation protocols of the Fig. 2 to 5, respectively. The results from the SDBS technique are also indicated (Fig. 6)

Table 2 Evaluation of the desynchronization within population 2 during stimulation ($t \in [20, 45]$) in the presence of (strong) global and (strong) local coupling

	Averaged Stimulation current	Mean Kuiper index (pop. 2)	Mean R (pop. 2)
Local coupling	1.2×10^{-5}	−0.455	0.094
Strong local coup.	1.2×10^{-5}	−0.279	0.070
Global coupling	1.3×10^{-5}	−0.470	0.094
Strong global coup.	1.4×10^{-5}	−0.528	0.098

The stimulation protocol is the same as used for Fig. 2. Parameters: coupling within population 1: $\bar{g}_s = 0.4$ (normal), $\bar{g}_s = 0.8$ (strong)

currents. The improved performance is due to the fact that in the second protocol, the LFP is measured in population 2 and in the third protocol the second population is stimulated itself, which results in a more direct stimulation of the second population where the effectiveness of the stimulation is calculated.

The third stimulation protocol (from Fig. 4) uses a nearly two times smaller amount of stimulation current while the effectiveness of the stimulation is the same as in the first protocol (Fig. 2). This means, even though the stimulation is repetitively effective during short periods only which are intersected by measurement periods, the resulting desynchronization remains the same. In contrast, SDBS (Fig. 6) requires a much larger stimulation current, and the resulting desynchronization is comparably weak. A comparison of the third stimulation protocol and SDBS shows that the standard high-frequency stimulation requires a 40 times larger amount of stimulation current with poor desynchronizing performance (the mean p-value of the Kuiper test is 1.6 times smaller and the mean synchronization measure is 1.3 times larger). Our technique works equally well in the case of strong global coupling, see Table 2.

Hence, the stimulation technique using delayed feedback at four different stimulation sites (Fig. 4) is clearly superior to the standard high-frequency stimulation technique (Fig. 6).

4 Discussion

In this paper we present for the first time a spatio-temporal control technique for robust desynchronization: A novel spatially coordinated delayed feedback causes an effective desynchronization of networks of coupled neurons. The measured and band-pass filtered LFP is fed back via several sites with different delays, respectively. The technique requires the use of at least two stimulation sites. For medical applications, all stimulation sites can be located in one depth electrode as will be demonstrated in a forthcoming study. The results indicate that the method is very robust and shows a very effective demand-controlled desynchronization even in the case of global coupling. Spatially incoherent noise sources are taken into account. However, desynchronization is induced even in the absence of noise.

Our novel technique establishes a long-lasting desynchronization, where minimal stimulation currents are necessary, even in the case of strong synaptic interactions. Our method makes it possible to perform a desynchronization which is as robust as that achieved by a coordinated reset via several sites [see below, cf. (Tass 2003a)]. An effective desynchronization with a coordinated reset requires repetitive administration of electrical shocks in a periodical or demand-controlled way (Tass 2003a). Consequently, the target population repetitively bounces between complete desynchronization and residual synchronized states (Tass 2003a). This is what makes our novel technique superior: The coordinated delayed feedback via several sites maintains an optimum of desynchronization without intermittent resynchronization and without repetitive artificial shock-like inputs into the target area. The next step in a more realistic modeling to investigate synchronization processes is to add the ability of the model to show different activity patterns, e.g. bursting, tonic firing, silence, depending on the current state of the population. The transitions might be induced by mechanisms like spike-time dependent plasticity, LTP or LTD, which will be investigated in a forthcoming study. In this study to simplify things we restricted ourselves to the bursting case, which promotes the entrainment of rhythmic activity.

In Sect. 3 we have shown that our desynchronizing stimulation technique also works effectively when applied to a driven population and not to the pacemaker directly. This finding is important for medical applications for two reasons. We can apply our stimulation technique even if the pacemaker cannot be targeted directly for surgical reasons, e.g., if electrode trajectories would damage arteries (causing severe cerebral bleedings). By the same token, our stimulation technique can be applied even if the pacemaker, underlying a particular pathology, has not yet been identified or if the pacemaker is not confined to one particular neuronal population.

Our results show that our novel stimulation technique is clearly superior to SDBS, with respect to both desynchronizing effect and energy consumption (Sect. 3): The mean stimulation current is 40 times larger for SDBS compared to our technique. Furthermore, SDBS hardly desynchronizes the synchronized activity, and SDBS induces alterations of the firing pattern. To understand this phenomena we shall shortly be performing a detailed theoretical study. Moreover, excellent animal model for investigating how stimulation induces transitions between bursting and firing might be the electroreceptors of paddle fish (Neiman and Russell 2004).

Delayed feedback control techniques were first developed by Pyragas (1992). Recently, the idea of Pyragas was extended to achieve a desynchronization in ensembles of coupled oscillators by Rosenblum and Pikovsky (2004). They found that in the parameter plane there are islands of desynchronized dynamics surrounded by a large sea of stimulus-induced synchronization (Yeung and Strogatz 1999). From the medical standpoint this means that a time consuming calibration and precise choice of stimulation parameters is mandatory. Furthermore, the method by Rosenblum and Pikovsky requires that the system parameters undergo at most minor variations. This aspect has to be considered as a severe limitation for medical applications. In Parkinson's disease, essential tremor and epilepsy, one typically observes variations of the mean frequency over time of up to 25% and even more (Nini et al. 1995). Consequently, with a fixed delay in Rosenblum's and Pikovsky's method, the system will vary between desynchronization and stimulus-induced synchronization (i.e., between the small islands and the surrounding sea). In other words, given the realistic variability of system parameters an experimentalist will run the risk of boosting the pathological rhythm instead of desynchronizing it. In contrast, our technique presented here effectively desynchronizes without preceding calibration over a wide range of model parameters, especially if the polarity of two of the four stimulation signals is changed as proposed in Tass (2003a). Our novel stimulation technique is very robust and works on demand which makes it predestined for clinical applications to diseases characterized by abnormal synchronization, e.g. to Parkinsonian tremor, essential tremor and epilepsy. As yet, the pathophysiology of akinesia and rigidity in PD is not fully understood. Abnormal synchronization in the beta-frequency band appears to be related to akinesia and rigidity (Brown et al. 2001) and might in that case be accessible to the approach presented here. In fact, novel control techniques might contribute to both an improvement of therapeutic procedures and a better understanding of the pathophysiology of diseases.

References

Alberts WW, Wright EJ, Feinstein B (1969) Cortical potentials and parkinsonian tremor. Nature 221:670–672

Batschelet E (1981) Circular statistics in biology. Academic Press, London

Benabid AL, Benazzous A, Pollak P (2002) Mechanisms of deep brain stimulation. Movement Disorders 17:73–74

Benabid AL, Pollak P, Gervason C, Hoffmann D, Gao DM, Hommel M, Perret JE, de Rougemount J (1991) Longterm suppression of tremor by chronic stimulation of ventral intermediate thalamic nucleus. The Lancet 337:403–406

Brown P, Oliviero A, Mazzone P, Insola A, Tonali P, Lazzaro VD (2001) Dopamine dependency of oscillations between subthalamic nucleus and pallidum in Parkinson's disease. J Neurosci 21:1033–1038

Dolan K, Witt A, Spano ML, Neiman A, Moss F (1999) Surrogates for finding unstable periodic orbits in noisy data sets. Phys Rev E 59:5235–5241

Hauptmann C, Mackey MC (2003) Stimulus dependent onset latency of the inhibitory recurrent activity. Biol Cybern 88:459–467

Hellwig B (2000) A quantitative analysis of the local connectivity between pyramidal neurons in layers 2/3 of the rat visual cortex. Biol Cybern 82:111–121

Kuiper NH (1960) Test concerning random points on a circle. Proc K Ned Akad Ser A: Math Sci 63:38–47

Kuramoto Y (1984) Chemical oscillations, waves, and turbulence. Springer, Berlin Heidelberg New York

Morris C, Lecar H (1981) Voltage oscillations in the barnacle giant muscle fiber. Biophys J 35:193–213

Neiman AB, Russell DF (2004) Two distinct types of noisy oscillators in electroreceptor of paddelfish. J Neurophysiol 92:492–509

Nini A, Feingold A, Slovin H, Bergmann H (1995) Neurons in the globus pallidus do not show correlated activity in the normal monkey, but phase-locked oscillations appear in the MPTP model of parkinsonism. J Neurophysiol 74:1800–1805

Nunez PL (1981) Electric Fields of the brain. Oxford University Press, New York.

Pinsky PF, Rinzel J (1995) Synchrony measures for biological neural networks. Biol Cybern 73:129–137

Pyragas K (1992) Continuous control of chaos by self-controlling feedback. Phys Lett A 170:421–428

Richardson K, Gluckman BJ, Weinstein SL, Glosch CE, Moon JB, Gwinn RP, Gale K, Schiff SJ (2003) In vivo modulation of hippocampal epileptiform activity with radial electric fields. Epilepsia 44:768–777

Rinzel J, Ermentrout GB (1989) Analysis of neural excitability and oscillations. In: Koch CH, Segev I (eds) Methods in neuronal modelling from synapses to networks, MIT, Cambridge, MA, pp 135–169

Rosenblum MG, Pikovsky AS (2004) Controlling synchronization in an ensemble of globally coupled oscillators. Phys Rev Lett 92:114102

Tass PA (1999) Phase resetting in medicine and biology. Springer, Berlin Heidelberg New York

Tass PA (2002a) Desynchronization of brain rhythms with soft phase-resetting techniques. Biol Cybern 87:102–115

Tass PA (2002b) Effective desynchronization with bipolar double-pulse stimulation. Phys Rev E 66:036226

Tass PA (2003a) A model of desynchronizing deep brain stimulation with a demand-controlled coordinated reset of neural subpopulations. Biol Cybern 89:81–88

Tass PA (2003b) Stochastic phase resetting of two coupled phase oscillators stimulated at different times. Phys Rev E 67:051902

Tass PA, Russell DF, Barnikol U, Neimann A, Yakusheva T, Hauptmann C, Voges J, Sturm V, Freund H-J (2005) Selective disruption of neural synchronization by means of repeated transient phase reset. (submitted)

Terman D, Rubin JE, Yew AC, Wilson CJ (2002) Activity patterns in a model for the subthalamopallidal network of the basal ganglia. J Neurosci 22:2963–2976

Traub RD, Miles R (1991) Neural networks of the hippocampus. Cambridge University Press, Cambridge

Volkmann J (2004) Deep brain stimulation for the treatment of parkinson's disease. J Clin Neurophysiol 21:6–17

Volkmann J, Joliot M, Mogilner A, Ioannides AA, Lado F, Fazzini E, Ribary U, Llinás R (1996) Central motor loop oscillations in parkinsonian resting tremor revealed by magnetoencephalography. Neurology 46:1359–1370

Yeung MKS, Strogatz SH (1999) Time delay in the Kuramoto model of coupled oscillators. Phys Rev Lett 82:648–651